Analysis of the Chatter Instability in a Nonlinear Model for Drilling

Sue Ann Campbell
Department of Applied Mathematics,
University of Waterloo, Waterloo, ON N2L 3G1 Canada

Emily Stone
Department of Mathematical Sciences,
The University of Montana, Missoula, MT 59812 U.S.A.

Abstract

In this paper we present stability analysis of a nonlinear model for chatter vibration in a drilling operation. The results build our previous work [1, 2], where the model was developed and the nonlinear stability of the vibration modes as cutting *width* is varied was presented. Here we analyze the effect of varying cutting *depth*. We show that qualitatively different stability lobes are produced in this case. We analyze the criticality of the Hopf bifurcation associated with loss of stability and show that changes in criticality can occur along the stability boundary, resulting in extra periodic solutions.

Keywords: delay differential equations, chatter, drilling, centre manifold reduction

INTRODUCTION

In a metal cutting operation such as turning, a cutting tool is directed perpendicularly to the cylindrical workpiece that is spinning along its longitudinal axis (the spindle), shaving a thin piece of material (a chip) as the spindle turns. Milling involves a similar local geometry, though multiple teeth in a cogged cutting tool shave a chip off a stationary work piece as they revolve. Drilling is more difficult to describe owing to the complex geometry of the drill bit, but at the bottom of the drill the cutting edges also revolve in the hole and remove a thin chip of material as they go. The twisted grooves in the side of the drill bit are there to direct the cut chip up and out of the hole being drilled. Understanding metal cutting and predicting optimal operating conditions has been a preoccupation of industrial engineers for the past 100 years, and lately high-speed machining and machining composites have renewed interest in the science of metal removal. In the aircraft industry drilling holes and filling them comprises a large part of the effort in manufacturing aircraft, so any gains in drilling technology are subsequently amplified.

Chatter in metal cutting is a vibration that is initiated by imperfections in the material being cut, and is maintained by the periodic driving force created from the oscillating thickness of the chip. Typically the cutting process is modeled as a spring-mass system, with the stipulation that the cutting force varies with chip thickness, and hence depends not only on the position of the cutting tool at a given time, but the position of the tool at the previous revolution of the workpiece. This leads to a delay term in the applied force on the oscillator, and chatter in metal cutting operations has been successfully described and predicted by delay differential equations. Tlusty and Tobias were the original pioneers of this work [3], see also studies by Stépán, Altintas, Bayly [4–8].

In this paper we investigate the chatter instability in a model of metal cutting relevant to drilling operations. In a previous paper [1] the derivation of the model is presented along with linear stability calculations for the onset of chatter. In another paper [2] we document the nonlinear stability of chatter in this model, using approximate center manifold techniques [9–12]. In both instances the instability parameter is proportional to the width of cut, the chatter commences as the cutting width is increased past a critical value, sometimes below the linear stability value, if the bifurcation is subcritical. Here we extend this study to include the effect of varying the cutting depth instead of cutting width, a reasonable parameter from the stand-point of the physical process. The depth of cut in drilling is controlled by the feed or the feed rate for the drill, which is determined by the force with which the drill is in contact with the material. Linear

stability boundaries are calculated for parameters similar to those used in the drilling models studied previously, and the nonlinear stability of the resulting oscillations is found via an approximate center manifold, computed using a symbolic algebra implementation based on the work of Campbell and Bélair [9]. We conclude with studies, using the branch following package DDE-BIFTOOL [13], of the periodic orbits (stable and unstable) and numerical simulations to illustrate the results.

In the remainder of this section we present background material from machining literature, a sketch of the stability analysis of DDEs with constant delay, and an overview of our previous results. In section two we present the linear and nonlinear analysis of the model with cutting depth as a bifurcation parameter, while varying cutting width. We conclude in section 3 with a discussion of these results as they relate to the earlier analysis, and to future work.

Chatter Vibrations and DDEs

Chatter has been modeled as the excitation of linear modes of vibration by the metal cutting force. If the force is directed perpendicular to the workpiece the process is known as "orthogonal cutting". The vibration modes are determined for the entire apparatus and the frequency and effective damping ratio of each mode is computed in laboratory tests. Generally only the lowest frequency modes are considered [14], and most commonly considered is a mode that vibrates up and down perpendicular to the workpiece. The equation of motion for this vibration mode excited by an orthogonal cutting force that depends on the thickness of the chip cut is:

$$m\frac{d^2y}{dt^2} + c\frac{dy}{dt} + ky(t) = F(f + y(t) - y(t-T)). \tag{1}$$

Here $y(t)$ is the vertical position of the tool, F is the thrust force on the tool (in the y direction) and depends on the chip thickness: $(f + y(t) - y(t-T))$ where f is the feed (how much the material is moved toward the tool) per revolution and T is the time required for one revolution. Thus the basic description is a linear mass-spring system (m being the mass, and k the spring constant) with viscous damping (c), being driven by a forcing function with a delay. Using conventional techniques the stability diagram for regenerative chatter can be created [14], we show an example in figure 1. The horizontal axis is spindle speed, which is inversely proportional to the delay, and the vertical axis is width of cut. Below the lobes the steady cutting solution is stable, upon crossing the boundary a complex conjugate pair of eigenvalues of the steady state crosses the

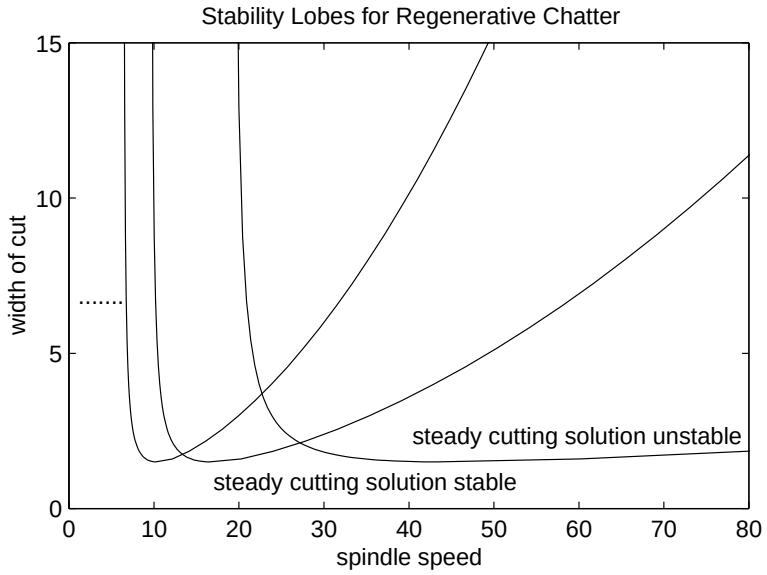

FIG. 1: Stability diagram for regenerative chatter. Steady cutting solution (the trivial solution) is stable in the region beneath the lobes.

imaginary axis and the stable fixed point becomes an unstable spiral. Similar stability diagrams can be found in the papers of [15–19], which consider a damped harmonic oscillator with delayed position and/or velocity dependent feedback.

The Drilling Model

In [1] we report a model for the excitation of two vibration modes seen in twist drills, the lowest frequency bending mode, which we called the "traditional mode", and a higher frequency axial-torsional mode thought to be the cause of striations formed on the bottom of the hole during high-speed drilling operations. The vibrations are assumed to be linear, with large inertia and stiffness, and small damping. The equation of motion in η, the modal amplitude, is hence:

$$m\ddot{\eta} + c\dot{\eta} + k\eta = F_\eta \tag{2}$$

where m is the inertial term, c is damping and k is stiffness. The forcing function, F_η depends on the chip width, w, and chip thickness, t_1, which are depicted in figure 2 and the geometry at the cutting surface, which is illustrated in figure 3. More specifically, F_η is the projection of the cutting force $\mathbf{R}$ onto the vibration direction (see figure 3) and $\mathbf{R}$ is determined from the Merchant-Oxley model of steady orthogonal cutting [20], [21].

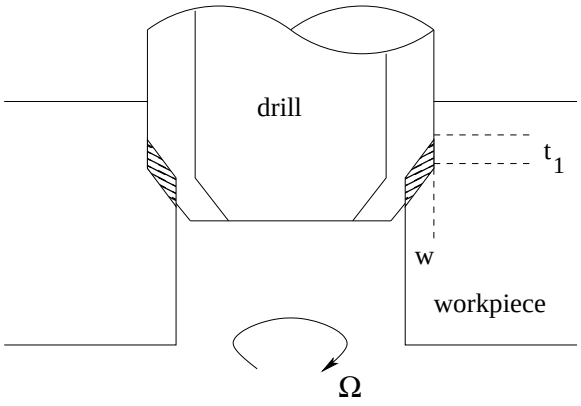

FIG. 2: Diagram of the drill geometry, showing the chip width, w, and the chip thickness (nominal cutting depth), t_1. Ω is the angular speed of the drill.

We also incorporated nonlinear friction of the chip sliding on the rake face of the tool, (through the friction coefficient λ). This friction force depends critically on the direction of the vibration mode in question, which is specified by the angle θ in figure 3. Other parameters are V, the cutting speed, ϕ, the shear plane angle, F_s, the force projected on the shearplane, and β the angle the shearplane makes with $\mathbf{R}$. (ϕ, F_s and β are used in the calculation of the cutting force, for more details see [1]).

The cutting force F_η is function of both η and $\dot{\eta}$, and takes the form:

$$F(\eta, \dot{\eta}) = w\tau(t_1 - \eta\cos\theta)(p_0 + p_1\dot{\eta} + p_2\dot{\eta}^2). \tag{3}$$

Note that the force depends on the instantaneous chip thickness $(t_1 - \eta\cos\theta)$ and the penetration rate, $\dot{\eta}$. In our calculations we used values typical of drilling aluminum: $\alpha = .26$, $w = 6.35 \times 10^{-3}$ m, $\tau = 276$ MPa, $k = 10^7$ N/m, $t_1 = 7.6 \times 10^{-5}$ m, $V = 400$ m/min, and a friction model that yielded expansion coefficients p_0, p_1, and p_2 in decreasing asymptotic order. The p's depend on cutting speed, rake angle and vibration angle in general. The sign of the p's depend critically on the vibration angle, both p_0 and p_1 are positive for the rake angles we considered in the case of the traditional vibration. The axial-torsional mode in question vibrates at an angle $\theta = 1.38 = 79^\circ$ relative to the vertical vibration of the traditional mode, a fact uncovered by three dimensional vibration analysis. In this case p_0 and p_1 are less than zero.

Including the effect of chip thickness variation introduces the delay, and in [1] and[2] we rescale time by the natural frequency of the undamped oscillator, and the amplitude by the cutting depth, t_1. This yields

$$\eta'' + \gamma\eta' + \eta - \beta(1 - (\eta - \eta_T)\cos\theta)(p_0 + \tilde{p_1}\eta' + \tilde{p_2}\eta'^2) = 0. \tag{4}$$

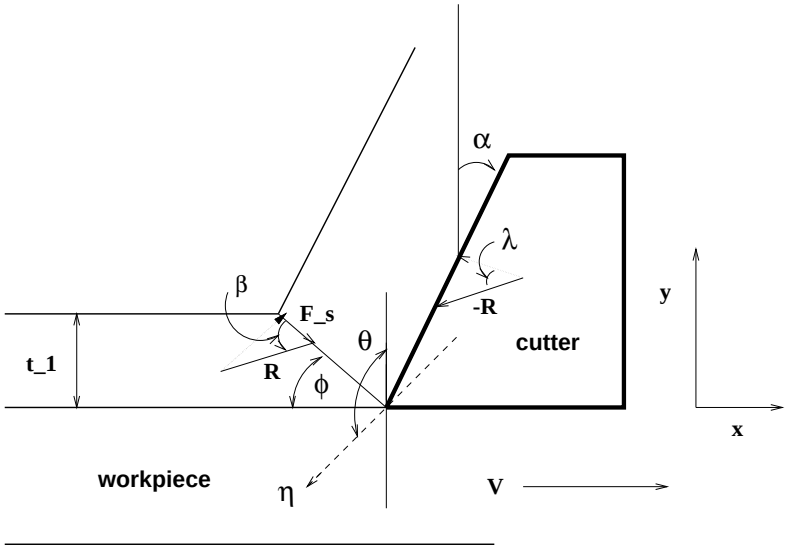

FIG. 3: Diagram of angles and forces for orthogonal cutting. The angle α is referred to as the rake angle, λ is the friction angle, ϕ is the shear plane angle. The cutting thickness is t_1, V is the cutting speed, R is the cutting force and F_s is the cutting force resolved along the shear plane.

where η is now the rescaled amplitude, and $\eta_T = \eta(t-T)$. Note that $1/T$ is spindle speed in revolutions per unit time, and η is now the rescaled amplitude variable, and η' is the derivative with respect to the rescaled time variable. From the non-dimensionalization we have $\beta = w\tau/k$ and $\tilde{p}_1, \tilde{p}_2$ are the rescaled p_1, p_2 (p_0 is left unchanged by the rescaling).

Linear and Nonlinear Stability Background

Equations such as (4) and many other models for metal cutting can be written in the following form, after translating the equilibrium point to the origin,

$$\eta''(t) + \delta_1\eta'(t) + \eta(t) + \delta_2(\eta(t) - \eta(t-T)) = f(\eta(t) - \eta(t-T), \eta'(t)), \tag{5}$$

where f is a nonlinear function and the δ_j depend on various physical parameters in the system. For example, when (4) is written in the form (5) then $\delta_1 = \gamma - \beta\tilde{p}_1$ and $\delta_2 = \beta p_0 \cos\theta$. We shall see in section 2 that using a different rescaling of the variables still yields an equation of the form (5) but with different expressions for the δ_j.

To study the linear (or local) stability of the equilibrium point we consider the lin-

earization of the model (5)

$$\eta''(t) + \delta_1\eta'(t) + \eta(t) + \delta_2(\eta(t) - \eta(t-T)) = 0. \tag{6}$$

As is the case for ordinary differential equations, solutions of this linear delay differential equation may be expressed in the form $\eta(t) = \kappa e^{\lambda t}$, where $\kappa, \lambda \in \mathcal{C}$. Some simple algebra shows that such solutions will exists if and only if λ is a root the characteristic equation

$$\lambda^2 + \delta_1\lambda + 1 + \delta_2(1 - e^{-\lambda T}) = 0. \tag{7}$$

Note that due to the delay, this is a transcendental equation in λ, which means it will have a countable infinity of complex roots. Nevertheless, it can be shown [22, 23] that the stability results from ordinary differential equations hold here as well. Specifically, if all the roots of (7) have $Re(\lambda) < 0$ then the equilibrium point is locally asymptotically stable and if at least one root has $Re(\lambda) > 0$ the the equilibrium point is unstable.

In a physical problem, one is, of course, interested in the dependence of the stability on the parameters of the system. Using techniques from complex variable theory and continuity arguments, one can describe regions of parameter space where all the roots of the characteristic equation have negative real parts. This is usually called the stability region of the equilibrium point.

In the study of chatter, we are particularly interested in determining the parameter values where the equilibrium point loses stability, this corresponds to parameter values where there is at least one root of (7) that satisfies $Re(\lambda) = 0$. Such points are said to define the boundary of the region of stability of the equilibrium point, or the stability boundary. These points can be found by putting $\lambda = 0$ or $\lambda = i\omega$ into the characteristic equation. For chatter problems, the former does not generally occur for physically meaningful parameter values. The latter, however, gives rise to the following (after separating into real and imaginary parts)

$$1 - \omega^2 + \delta_2(1 - \cos\omega T) = 0 \tag{8}$$

$$\delta_1\omega + \delta_2 \sin\omega T = 0. \tag{9}$$

These can be further rearranged to give an equation for T as a function of ω and the other parameters:

$$T = \frac{2}{\omega}\left(\arctan\left(\frac{1-\omega^2}{\delta_1\omega}\right) + N\pi\right), \tag{10}$$

where $N = 0, 1, 2, \ldots$ determines the branch of the arctangent function, and another equation which is independent of T

$$(1 - \omega^2 + \delta_2)^2 + \delta_1^2\omega^2 - \delta_2^2 = 0. \tag{11}$$

From this last equation, we can solve for one of the physical parameters as a function of ω and the other parameters. For example, if (11) is derived from the model (4), one can solve for β in terms of the other parameters, since $\delta_1 = \gamma - \beta\tilde{p}_1$ $\delta_2 = \beta p_0 \cos\theta$.

For our general set up, let μ be the physical parameter we solve for. Thus, for fixed values of the other parameters, (10)–(11) yield parametric equations, $T = T(\omega)$, $\mu = \mu(\omega)$, describing curves in the T, μ parameter space. Along these curves, the characteristic equation has a pair of pure imaginary roots, thus one may expect that a Hopf bifurcation occurs. To show that this is indeed the case, one needs to check the transversality and nonresonance conditions of the Hopf bifurcation Theorem for DDEs [22, pp.331-333]. These conditions may be checked via manipulation of the characteristic equation, (7). For an example, see the appendix of [2].

Assuming that a Hopf bifurcation does take place as either T or μ is varied through the curves described by (10)–(11), we now discuss how to determine whether this is a supercritical or subcritical bifurcation.

To study the criticality of the Hopf bifurcation, it is useful to rewrite the model (5) as a first order system, viz.,

$$\mathbf{x}'(t) = A_0\mathbf{x}(t) + A_1\mathbf{x}(t-T) + \mathbf{f}(\mathbf{x}(t), \mathbf{x}(t-T)) \tag{12}$$

where

$$\mathbf{x}(t) = \begin{bmatrix} \eta(t) \\ \eta'(t) \end{bmatrix}, \; A_0 = \begin{bmatrix} 0 & 1 \\ -(1+\delta_2) & -\delta_1 \end{bmatrix}, \; A_1 = \begin{bmatrix} 0 & 0 \\ \delta_2 & 0 \end{bmatrix}, \tag{13}$$

and

$$\mathbf{f} = \begin{bmatrix} 0 \\ f(x_1(t) - x_1(t-T), x_2(t)) \end{bmatrix}. \tag{14}$$

The linearization of this equation about the trivial solution is

$$\mathbf{x}'(t) = A_0\mathbf{x}(t) + A_1\mathbf{x}(t-T). \tag{15}$$

It can be shown [22] that the solution space of equations such as (12) and (15) is infinite dimensional and thus the appropriate phase space for (12) is $\mathcal{C} \stackrel{def}{=} C([-T, 0], \mathbb{R}^2)$, the space of continuous functions mapping the interval $[-T, 0]$ into $\mathbb{R}^2$. The equation may be recast in terms of this phase space by defining the function

$$\mathbf{x}_t(\sigma) \stackrel{def}{=} \mathbf{x}(t+\sigma), \; -T \leq \sigma \leq 0,$$

to be the "phase point" at time t. Note that this represents the value of the state $\mathbf{x}$ at time t together with its past history to $t - T$.

Despite the infinite dimensionality of this phase space, many of the properties of solutions of delay differential equations such as (12) are similar to those for ordinary differential equations [22]. In particular, at a Hopf bifurcation point, there exists a two dimensional centre manifold in the solution space. Further, if all the other roots of the characteristic equation of the linearization about the equilibrium have negative real parts, then the centre manifold is attracting and the long term behaviour of solutions to the nonlinear delay differential equation is well approximated by the flow on this manifold. As discussed in [9–12] the criticality of the Hopf bifurcation can be determined by studying the evolution of solutions on the centre manifold. We note that since the manifold is finite dimensional, this evolution will be described by a system of ordinary differential equations. In the following we will outline the steps needed to find this system of ordinary differential equations. Details of the computations for (4) and the theory behind them can be found in the appendix of [2].

A standard result from the theory of DDEs [22] indicates that the characteristic equation (7) has at most a finite number of roots with positive real parts. Thus at points along the curves described by (10)–(11), the trivial solution of (12) has a two dimensional "centre eigenspace", N, with basis

$$\mathbf{\Phi}(\sigma) = [\phi_1(\sigma), \phi_2(\sigma)] = \begin{bmatrix} \cos(\omega\sigma) & \sin(\omega\sigma) \\ -\omega\sin(\omega\sigma) & \omega\cos(\omega\sigma) \end{bmatrix}, \tag{16}$$

an infinite dimensional "stable eigenspace", S, and a finite dimensional "unstable eigenspace", U.

The corresponding centre manifold is given by

$$M_f = \{\phi \in \mathcal{C} \mid \phi = \mathbf{\Phi}\mathbf{u} + \mathbf{h}(\mathbf{u})\},$$

where $\mathbf{u} = [u_1, u_2]^T$ are coordinates on N and $\mathbf{h}(\mathbf{u}) \in S \oplus U$. Solutions to the DDE (12) on M_f are given by $\mathbf{x}_t(\sigma) = \mathbf{\Phi}(\sigma)\mathbf{u}(t) + \mathbf{h}(\sigma, \mathbf{u}(t))$, which can be expressed as

$$\begin{aligned} \mathbf{x}_t(\sigma) \;=\; & \begin{bmatrix} \cos(\omega\sigma)u_1(t) + \sin(\omega\sigma)u_2(t) \\ -\omega\sin(\omega\sigma)u_1(t) + \omega\cos(\omega\sigma)u_2(t) \end{bmatrix} \\ & + \begin{bmatrix} h^1_{11}(\sigma)u_1(t)^2 + h^1_{12}(\sigma)u_1(t)u_2(t) + h^1_{22}(\sigma)u_2(t)^2 \\ h^2_{11}(\sigma)u_1(t)^2 + h^2_{12}(\sigma)u_1(t)u_2(t) + h^2_{22}(\sigma)u_2(t)^2 \end{bmatrix} + \mathrm{O}(\|\mathbf{u}\|^3), \end{aligned}$$

where the $h^i_{jk}(\sigma)$ are found by solving an ODE boundary value problem as described in the appendix of [2].

The dynamics on the centre manifold are given by the evolution in time of the coordinates $u_1(t),\ u_2(t)$. This is governed by the system of ODEs

$$\begin{aligned}\dot{u}_1 &= \omega u_2 + \mathbf{\Psi}_{12}(0)(f_{11}u_1^2 + f_{12}u_1u_2 + f_{22}u_2^2 + f_{111}u_1^3 + f_{112}u_1^2u_2 + f_{122}u_1u_2^2 + f_{222}u_2^3) \\ \dot{u}_2 &= -\omega u_1 + \mathbf{\Psi}_{22}(0)(f_{11}u_1^2 + f_{12}u_1u_2 + f_{22}u_2^2 + f_{111}u_1^3 + f_{112}u_1^2u_2 + f_{122}u_1u_2^2 + f_{222}u_2^3)\end{aligned} +\mathrm{O}(\|\mathbf{u}\|^4).$$

The $\Psi_{ij}(0)$ are functions of the physical parameters of the system, and of the Hopf frequency, ω. The $f_{ij},\ f_{ijk}$ are functions of these and the centre manifold coefficients $h^i_{jk}(0)$ and $h^i_{jk}(-T)$.

Using the result given in [24, p. 152], it is easily shown that the criticality of the Hopf bifurcation is determined by the sign of the following quantity

$$\begin{aligned} a \ = \ & \frac{1}{8}\left[\mathbf{\Psi}_{12}(0)(3f_{111} + f_{122}) + \mathbf{\Psi}_{22}(0)(f_{112} + 3f_{222})\right] \\ & -\frac{1}{8\omega}\left[(\mathbf{\Psi}_{12}(0)^2 - \mathbf{\Psi}_{22}(0)^2)f_{12}(f_{11} + f_{22}) + 2\mathbf{\Psi}_{12}(0)\mathbf{\Psi}_{22}(0)(f_{22}^2 - f_{11}^2)\right]. \end{aligned} \tag{17}$$

If $a < 0$ then the Hopf bifurcation is supercritical and if $a > 0$ it is subcritical. If $a = 0$ the criticality is not determined by the third order terms of the equation.

Although these computations are long, they can be automated in a symbolic algebra package such as Maple [9]. From this one obtains an expression for a as a function of the physical parameters and the Hopf frequency, ω. This expression can then be evaluated at points along the curves described by (10)–(11), and in particular along the stability boundary, to determine if the Hopf bifurcation is super- or subcritical.

Overview of previous results

In [1] we determined linear stability boundaries for the drilling model for both the axial-torsional and traditional vibration mode. There we solved (4) for T and β as functions of ω, and in terms of these variables equations (11) and (10) are written

$$p_1^2\omega^2\beta^2 - ((\omega^2 - 1)(2p_0\cos\theta) + 2\gamma p_1\omega^2)\beta + (\gamma^2\omega^2 + (\omega^2 - 1)^2) = 0. \tag{18}$$

and

$$T(\omega) = \frac{2}{\omega}(\arctan(\frac{1 - \omega^2}{(\gamma - \beta p_1)\omega}) + N\pi). \tag{19}$$

For the axial-torsional case positive solutions for β occur for values of ω between zero and 1, and for the traditional case, for values of ω greater than 1, indicating that the

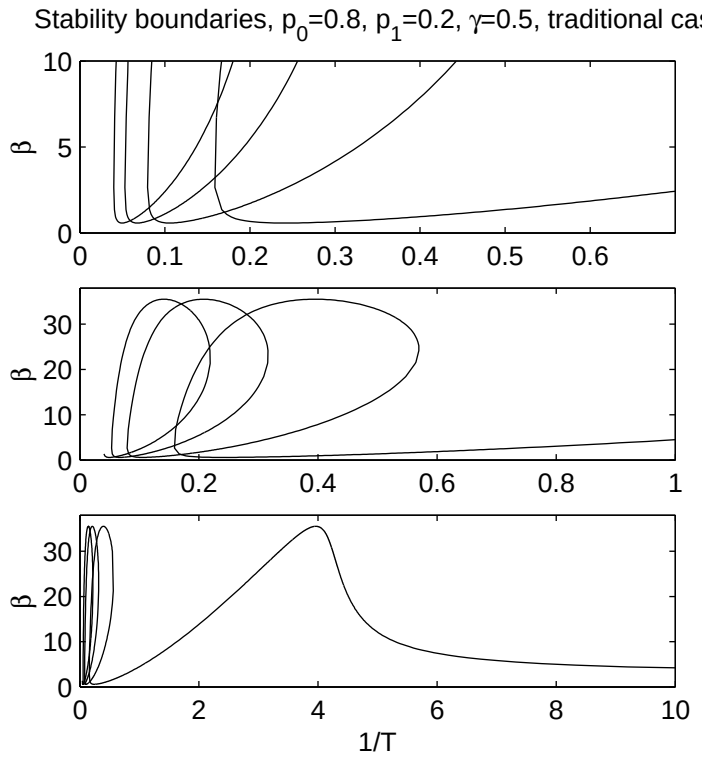

FIG. 4: Stability diagram for the traditional case: $\gamma = 0.5$, $p_0 \cos\theta = 0.8$, $\tilde{p}_1 = 0.2$. Moving from top to bottom zooms out from the area near the lower part of the boundary for lower cutting speeds. The trivial solution is unstable in the region above the boundaries, and stable below.

steady solution loses stability to a vibration with frequency above or below the natural frequency of the mode in question. Examples of these boundaries are shown in figures 4 and 5.

We evaluated the Hopf coefficient (17) along the boundary of the stability regions for both the traditional case and the axial-torsional case. In the traditional case, the Hopf bifurcation is subcritical for large values of T (small turning speeds) then switches to supercritical at some intermediate value of T and remains so for small values of T (large turning speeds). Increasing the damping moves the point of change of criticality to smaller values of T. The results are illustrated in figs. 6 and 7. Hatched lines denote subcritical Hopf bifurcation and dark lines supercritical. In the axial-torsional case, the Hopf bifurcation is always subcritical.

We also examined the high-speed limit where the delay differential equation becomes

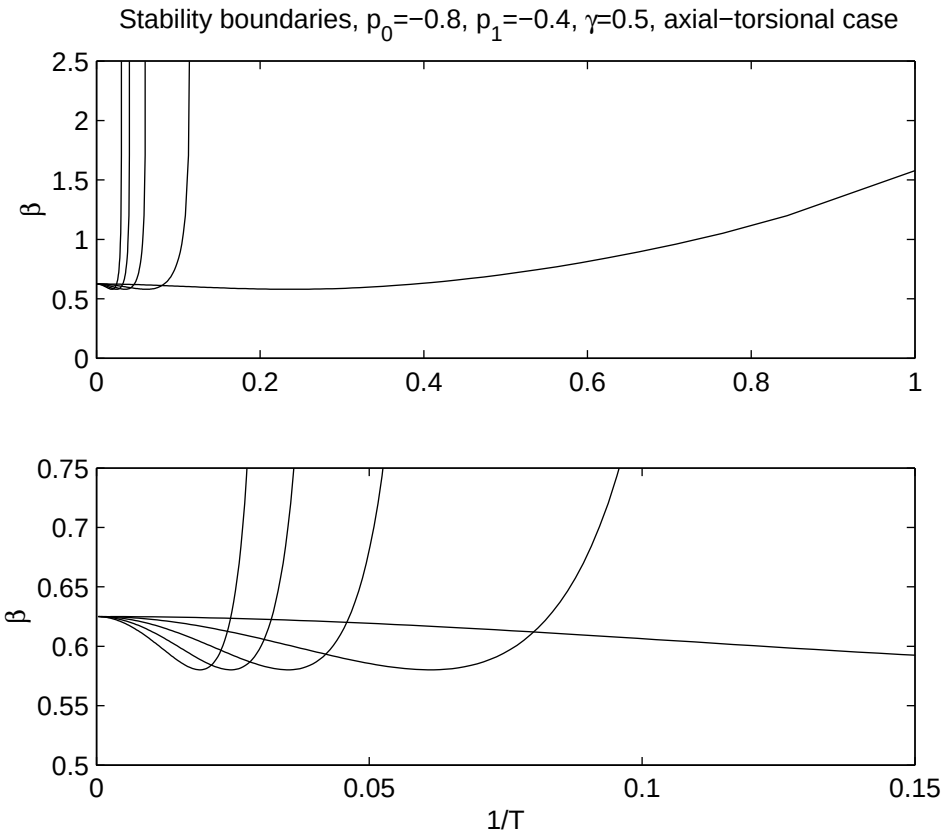

FIG. 5: Stability diagram for axial-torsional vibration: $\gamma = 0.5$, $p_0 \cos\theta = -0.8$, $\tilde{p}_1 = -0.4$. Moving from bottom to top zooms in on the area near the lower part of the boundary for lower cutting speeds. The trivial solution is unstable in the region above the boundaries, and stable below.

an ordinary differential equation that can be analyzed by conventional techniques. We found that the vector field for this system influences the structure of the flow in the small delay case, and that the criticality coefficient for the Hopf bifurcation is zero, indicating degeneracy. Numerical simulations of the delay differential equation in this limit show a global bifurcation leading to a large scale limit cycle whose period increases with increasing speed, reminiscent of a heteroclinic bifurcation in non-delayed systems.

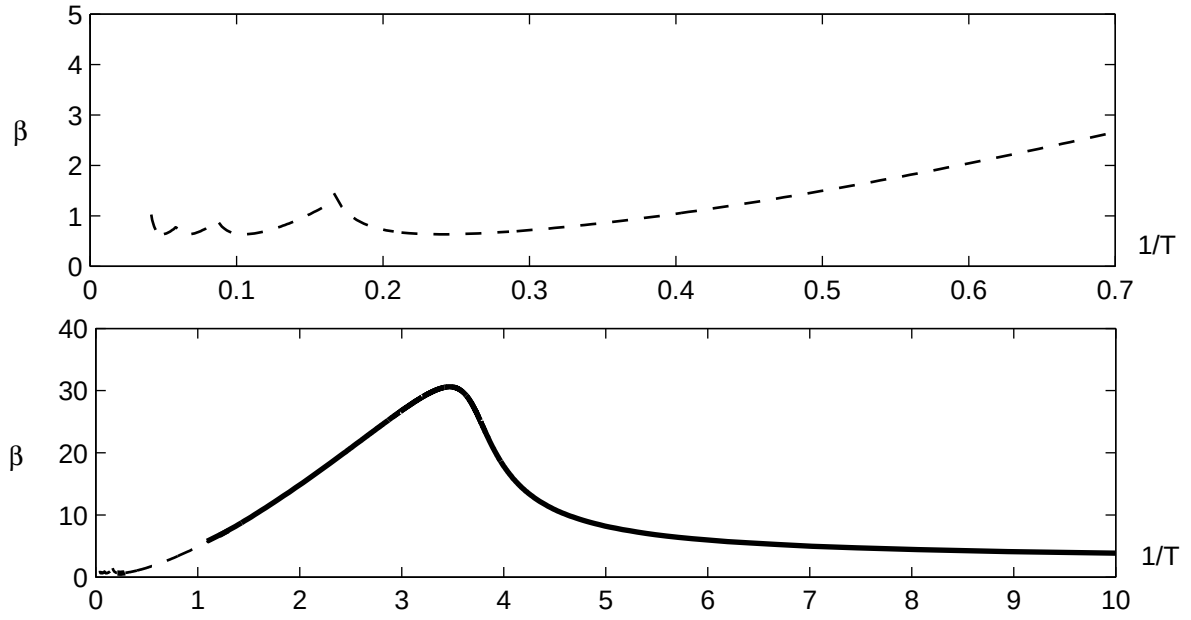

FIG. 6: Stability boundary showing criticality of Hopf bifurcation. The top diagram is a blow-up of the bottom diagram, and hatched lines indicate a subcritical Hopf bifurcation, solid lines a supercritical Hopf. Traditional case with $p_0\cos(\theta) = 0.8,\ \tilde{p}_1 = 0.2,\ \tilde{p}_2 = 0.1,\ \gamma = 0.5$.

STABILITY WITH RESPECT TO DEPTH OF CUT

In this section we present the derivation and analysis of the drilling model rescaled so that we can use the *depth* of cut, t_1, as the bifurcation parameter, rather than the *width* of cut, w.

The equation of motion prior to rescaling is obtained by combining equations (2) and (3) to yield

$$m\ddot{\eta} + c\dot{\eta} + k\eta = w\tau(t_1 - \eta\cos\theta)(p_0 + p_1\dot{\eta} + p_2\dot{\eta}^2). \tag{20}$$

After rescaling time with respect to the natural frequency of the undamped oscillator ($\omega_0 = \sqrt{\frac{k}{m}}$) we obtain

$$\eta'' + \gamma\eta' + \eta = \frac{w\tau}{k}(t_1 - \eta\cos(\theta))(p_0 + \tilde{p}_1\eta' + \tilde{p}_2\eta'^2) \tag{21}$$

where $\tilde{p}_1 = \omega_0 p_1$ and $\tilde{p}_2 = \omega_0^2 p_2$. The natural rescaling of the amplitude by t_1 is not done here, in order to examine the stability of the trivial solution with respect to the chip thickness.

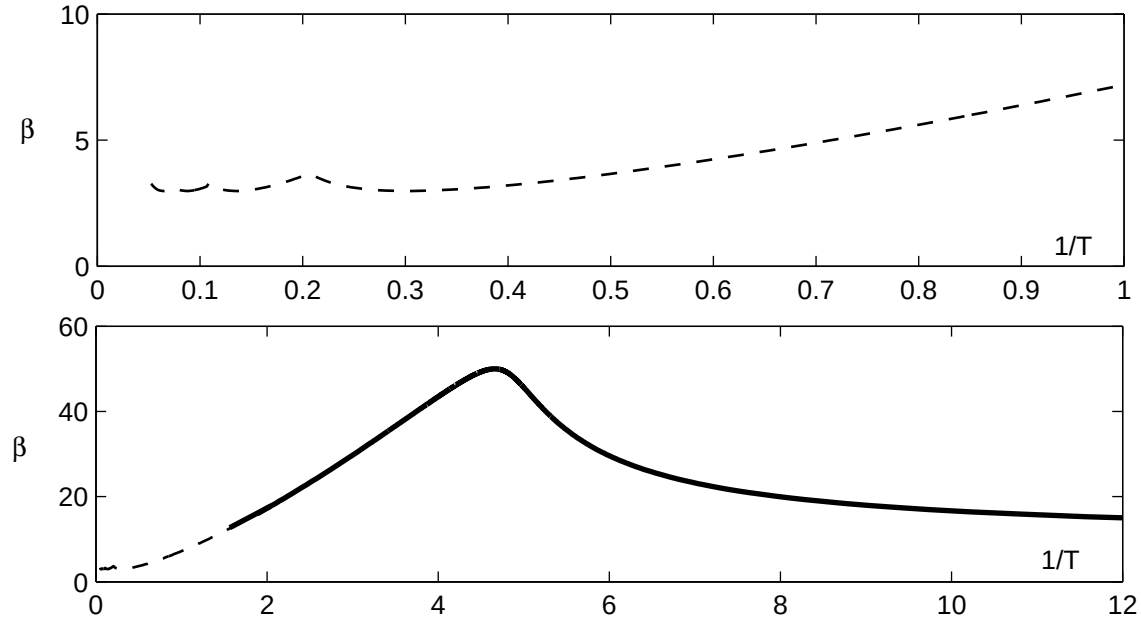

FIG. 7: Stability boundary showing criticality of Hopf bifurcation. The top diagram is a blow-up of the bottom diagram, and hatched lines indicate a subcritical Hopf bifurcation, solid lines a supercritical Hopf. Traditional case with $p_0\cos(\theta) = 0.8,\ \tilde{p}_1 = 0.2,\ \tilde{p}_2 = 0.1,\ \gamma = 2.0.$

Accounting for variation in chip thickness adds the delay, T, and we have

$$\eta'' + \gamma\eta + \eta = \frac{w\tau}{k}(t_1 - (\eta(t) - \eta(t-T))\cos(\theta))(p_0 + \tilde{p}_1\eta' + \tilde{p}_2\eta'^2). \tag{22}$$

Linearizing about the fixed point $\eta_0 = \beta t_1 p_0 \cos\theta$, where $\beta = \frac{w\tau}{k}$, and $z = \eta - \eta_0$ produces the following equation

$$z'' + (\gamma - \beta\tilde{p}_1 t_1)z' + z = -\beta p_0\cos(\theta)(z(t) - z(t-T)). \tag{23}$$

The linear stability curves are defined by the parametric equations

$$T(\omega) = \frac{2}{\omega}(\arctan(\frac{1-\omega^2}{(\gamma - \beta\tilde{p}_1 t_1)\omega}) + N\pi) \tag{24}$$

where $N = 0, 1, 2, ...$ counts the branches of the arctangent function, generating the separate lobes of the diagram. To solve for T, t_1 must first be found by solving the following quadratic equation (equation (11) with $\delta_2 = \beta p_0\cos\theta$, and $\delta_1 = \gamma - \beta\tilde{p}_1 t_1$),

$$(1 - \omega^2 + \beta p_0\cos\theta)^2 + (\gamma - \beta\tilde{p}_1 t_1)^2\omega^2 - (\beta p_0\cos\theta)^2 = 0. \tag{25}$$

Conditions for a real solution to this quadratic in t_1 determine allowable ranges of the parameter ω, and depend on the values of $\beta, \tilde{p_0}$ and γ. Specifically,

$$t_1^{\pm} = \frac{\gamma}{\tilde{p}_1\beta} \pm \frac{\sqrt{(\omega^2-1)(1+2\beta p_0\cos(\theta)-\omega^2)}}{\tilde{p}_1\beta\omega}, \tag{26}$$

so that t_1 will be a real valued-function of ω when either $\omega^2-1>0$ and $1+2\beta p_0\cos(\theta)-\omega^2>0$, or both when both expressions are <0. The former implies the range $1<\omega^2<1+2\beta p_0\cos(\theta)$, hence also requires that $p_0\cos(\theta)>0$, which occurs in the traditional vibration case. The latter set of inequalities combines to give $1+2\beta p_0\cos(\theta)<\omega^2<1$, which can be satisfied if $p_0\cos(\theta)<0$, which occurs in the axial-torsional vibration case. Plots of the stability boundaries in each case, for varying β, are shown in figures 8 and 9. The region below the $1/T$ axis is not physically relevant, since the cutting depth is negative there, we include it to show the structure of the loops.

In both cases the boundaries oscillate for smaller values of β, forming overlapping loops with increasing branch number N. The exact criteria for the loops will depend in a complicated manner on the interplay between the expression for $\frac{1}{T}$ and t_1 and will not be calculated here. We do note, however, that in the axial-torsional case the branches will diverge for large enough β. The critical value of β is given by the point when the lower boundary for ω, $1+2\beta p_0\cos\theta$, is zero, or $\beta_c=\frac{1}{2|p_0\cos\theta|}$. Then $\omega\to 0$ is the lower boundary and $t_1\to\pm\infty$ in this limit. This divergence is illustrated the bottom plots of figure 9.

From the small delay/large speed limit we can determine the stability of the region immediately above and below the entire boundary. The equation of motion in this case is simply

$$\eta''+\gamma\eta'+\eta=\beta t_1(p_0+\tilde{p}_1\eta'+\tilde{p}_2\eta'^2)$$

and the stability of the trivial solution is defined by the sign of linear damping term:

$$\gamma-\beta t_1\tilde{p}_1.$$

The $N=0$ branch will asymptote on the value $t_1=\frac{\gamma}{\beta\tilde{p}_1}$ in the limit as $\frac{1}{T}\to\infty$. which will be negative when $\tilde{p}_1<0$, positive when $\tilde{p}_1>0$. Above the boundary the damping will be positive if $\tilde{p}_1<0$, i.e. the axial-torsional case, and negative if $\tilde{p}_1>0$, in the traditional case. Consequently, the region above the zero-th branch will be stable to axial-torsional vibrations, and the region below it is stable to traditional vertical vibrations. By continuity the real parts of the roots of the quasi-polynomial (7) will be the same in that region until another branch is encountered, at which point a complex conjugate pair of roots crosses the imaginary axis. We note here that increasing cutting depth has the

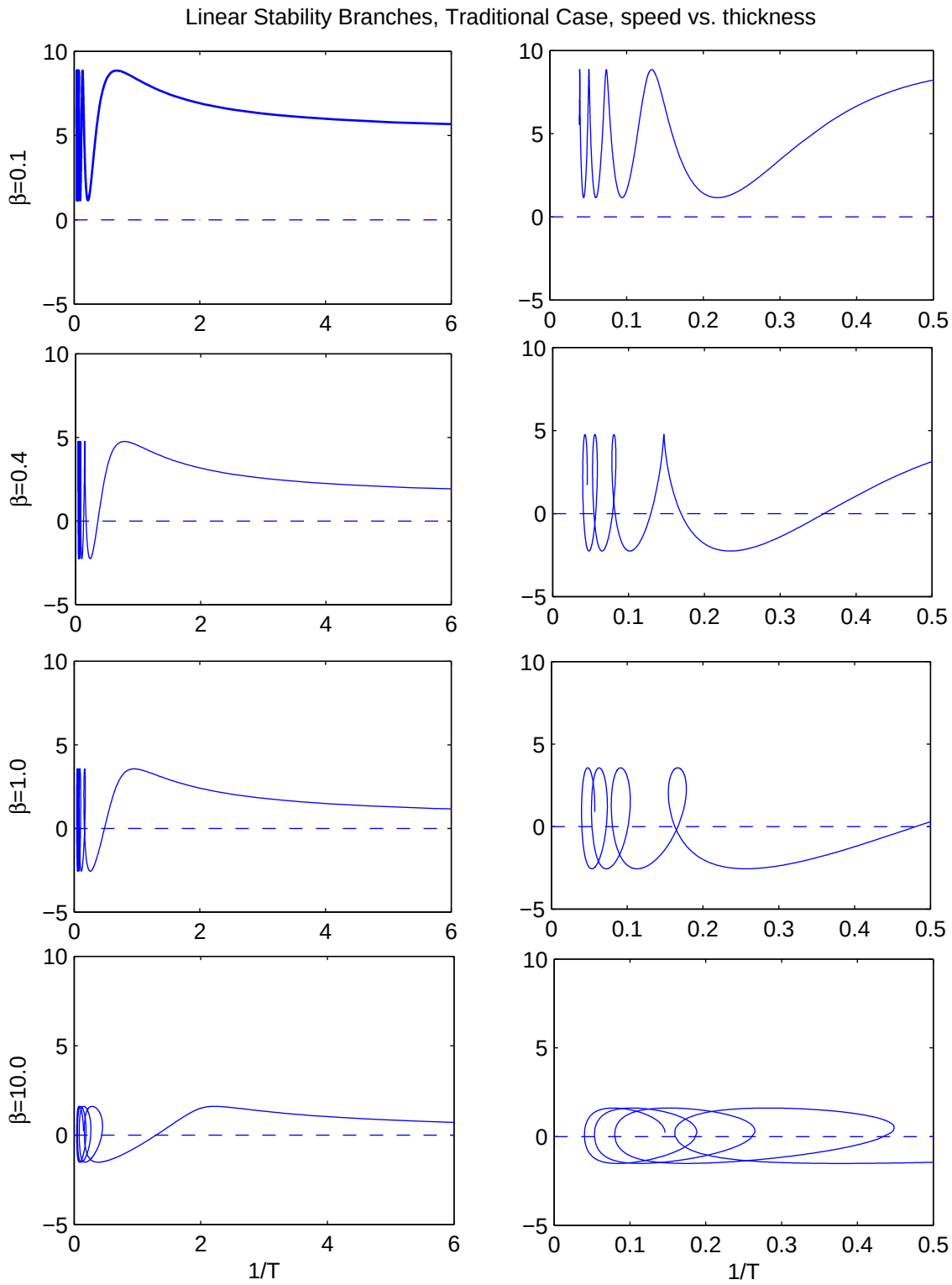

FIG. 8: Linear stability boundaries varying β, t_1 vs. $\frac{1}{T}$, traditional vibration parameters.

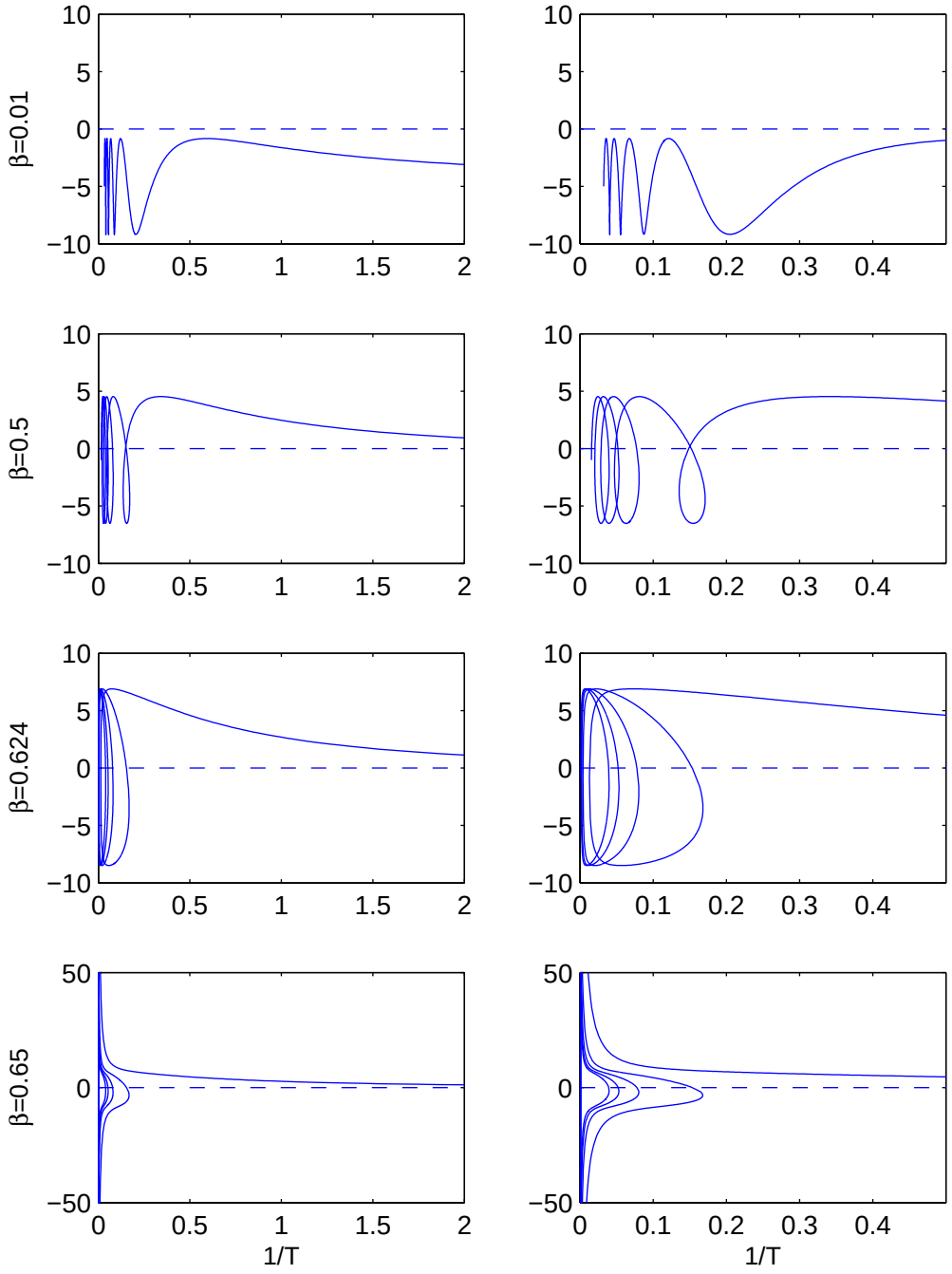

FIG. 9: Linear stability boundaries varying β, t_1 vs. $\frac{1}{T}$, axial-torsional vibration parameters.

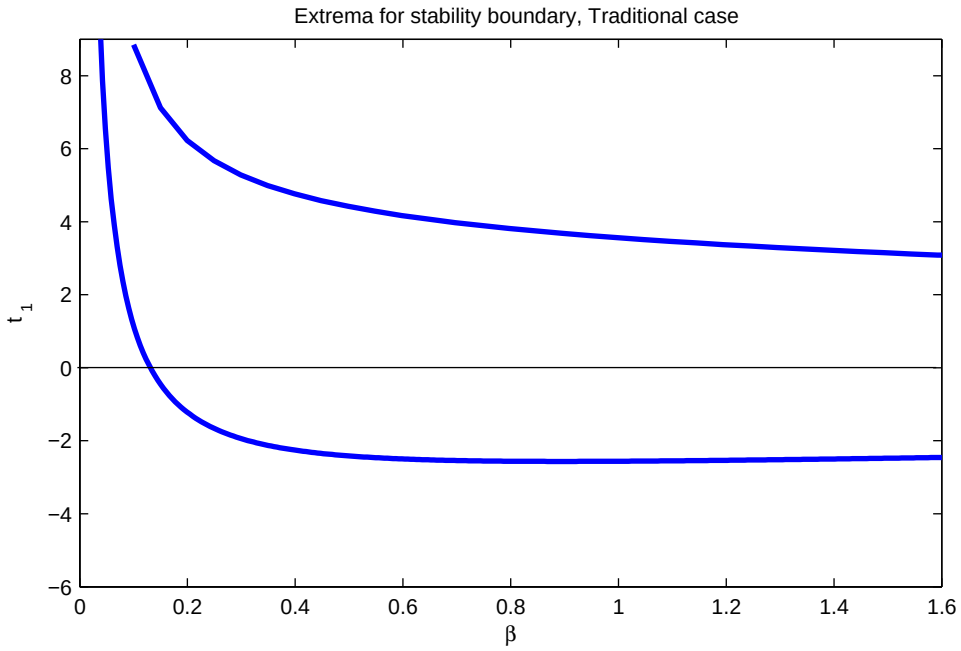

FIG. 10: Extrema envelope of t_1 boundary as function of β, traditional vibration parameters.

somewhat non-intuitive result of damping axial-torsional vibrations, consistent with the presence of t_1 in the linear damping term. The sign of the damping due to the nonlinear friction determines if increasing t_1 will be stabilizing or destabilizing.

It is clear from figures 8 and 9 that the maximum value of the lobes shifts with increasing β, up in the axial-torsional case, and down in the traditional case. This reflects the high-speed stability result, where increasing β decreases the region of stability, which is below the curve in the traditional case, and above the curve in the axial-torsional case. The minima follow the maxima until either they both tend toward zero (in the traditional case) or they diverge (in the axial-torsional case). This can be illustrated by computing the maximum and minimum values of the lobes as a function of β. To do so we first solve (25) for t_1 as a function of ω, where the plus root forms the top part of the lobes, and the minus root forms the bottom in the traditional case, vice versa in the axial-torsional case. To determine the extrema we solve for the critical points of each, ω_c, and evaluate t_1 at these points. For the plus t_1 branch this yields

$$t_{1crit} = \frac{\gamma A^{1/2} + \sqrt{2[A(1+\beta p_0 \cos\theta) - 1 - 2\beta p_0 \cos\theta]}}{\tilde{p}_1 \beta A^{1/2}} \tag{27}$$

where $A = \sqrt{1 + 2\beta p_0 \cos\theta}$. For the parameter values used in the traditional case the envelope comprised of both the maximum and the minimum values of the lobes varies

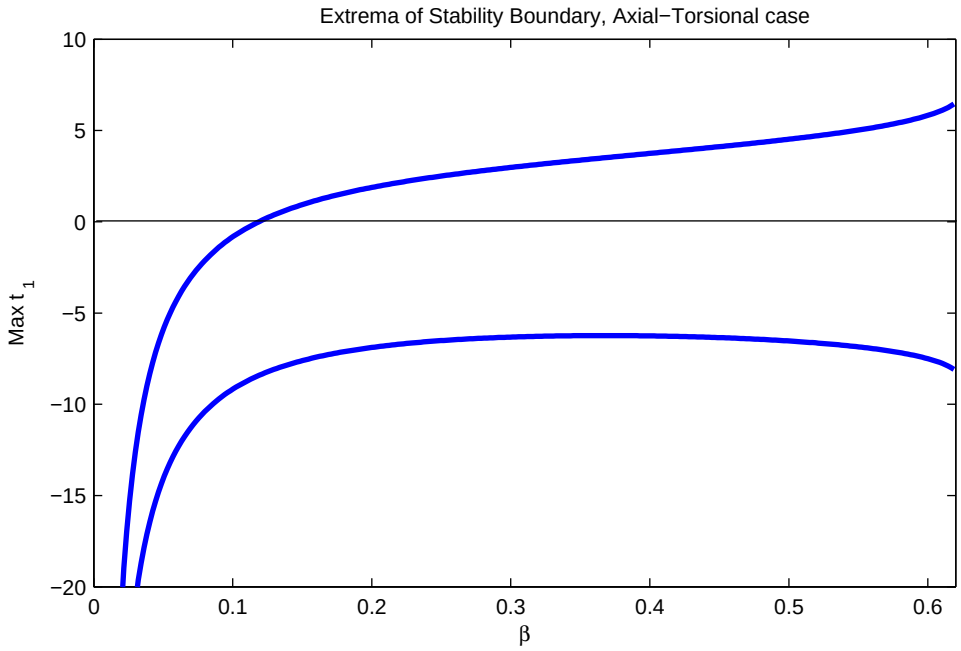

FIG. 11: Extrema envelope of t_1 boundary as function of β, axial-torsional vibration parameters.

with β according to the graph shown in figure 10, confirming the observation that the tops of the lobes move down with increasing β. In this case it is straight-forward to show that in the limit as β goes to zero both the maximum and minimum diverge, and as β goes to infinity they tend to zero.

In figure 11 the variation of both the maxima and minima of the lobes for the axial-torsional case is shown. Recall that for $\beta > \frac{1}{(2|p_0 \cos\theta|)}$ the boundary uncoils and the branches diverge to $\pm\infty$ as $\omega \to 0$, so no local maximum or minimum exist. For the parameter values in question this occurs when $\beta = 0.625$, at which point both expressions cease to exist, since $1 + 2\beta p_0 \cos\theta < 0$. It can be shown that as $\beta \to 0$ both the maxima and the minima tend to $-\infty$.

Nonlinear Stability

As discussed in section 1, along each of the curves shown in figures 8–9, the characteristic equation has a pair of pure imaginary eigenvalues. Some straightforward calculations show that, for fixed T, (22) undergoes a Hopf bifurcation as t_1 is varied through the curve. We also showed in section 1 that the criticality of this bifurcation is determined

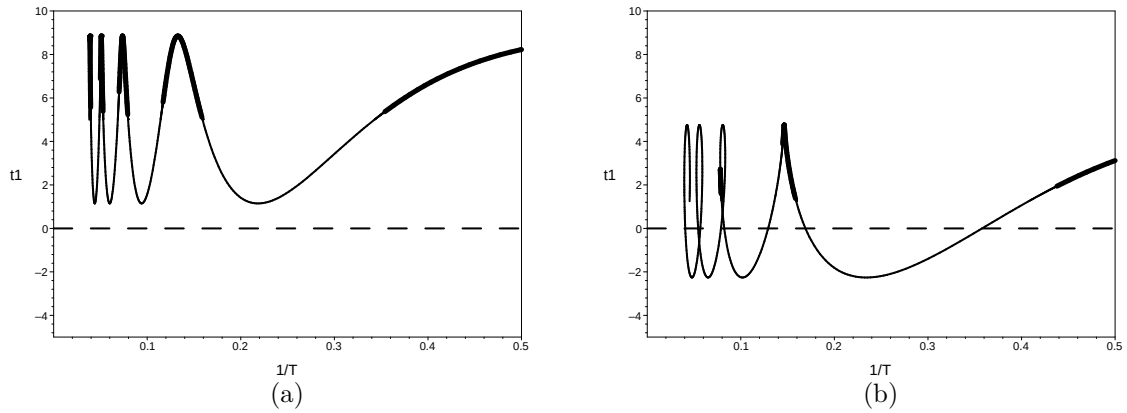

(a) (b)

FIG. 12: Stability boundary showing criticality of Hopf bifurcation in the traditional case for (a) $\beta = 0.1$ and (b) $\beta = 0.4$. Other parameter values are: $p_0 \cos(\theta) = 0.8$, $\tilde{p}_1 = 0.2$, $\tilde{p}_2 = 0.1$, $\gamma = 0.1$ Thin lines indicate a subcritical Hopf bifurcation, thick lines a supercritical Hopf.

by the coefficient a given by eq. (17). We calculated a using the symbolic algebra package Maple in a manner similar to that described in [2], and evaluated this coefficient along the curves defining the stability region for both the traditional case and the axial-torsional case.

In traditional case, the Hopf bifurcation is supercritical for small values of T (large turning speeds) then switches to subcritical at some intermediate value of T. After this it undergoes several switches from sub- to super-critical and back again. Fig. 12 shows a plot of the curves which define the stability boundary for $\beta = 0.1,\ 0.4$. Note that the lower parts of the lobes are subcritical while the upper parts are supercritical. As β is increased, more of each curve becomes subcritical.

In the axial-torsional case, the Hopf bifurcation is subcritical for small values of T (large turning speeds) then switches to supercritical at some intermediate value of T. After this it undergoes several switches from super- to sub-critical and back again. Fig. 13 shows a plot of the curves which define the stability boundary for $\beta = 0.1,\ 0.5$. Note that the lower parts of the lobes are supercritical while the upper parts are subcritical. As β is increased, more of each curve becomes subcritical. Note also that, other than at $\beta = 0.1$, the Hopf bifurcation appears to always be subcritical along the boundary of the stability region.

To verify these predictions we performed numerical simulations on the full model (22), with the equilibrium shifted to zero. The simulations were performed using the package

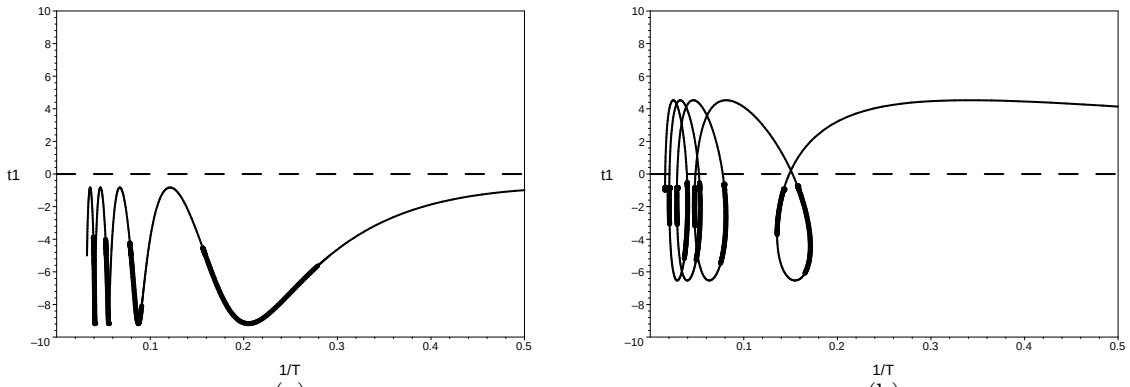

FIG. 13: Stability boundary showing criticality of Hopf bifurcation in the axial torsional case for (a) $\beta = 0.1$ and (b) $\beta = 0.5$. Other parameter values are $p_0 \cos(\theta) = -0.8$, $\tilde{p}_1 = -0.2$, $\tilde{p}_2 = -0.1$, $\gamma = 0.1$. Thin lines indicate a subcritical Hopf bifurcation, thick lines a supercritical Hopf.

XPPAUT [25] which uses a fourth order Runge-Kutta integrator adapted for delay differential equations. In all cases, the simulations confirmed our predictions. However, some simulations showed additional behaviour not predicted by our centre manifold calculations. For example, in fig. 14, we show simulations at a point where the Hopf bifurcation is predicted to be supercritical, but close to where it is predicted to change from from supercritical to subcritical. Before the bifurcation (fig. 14(a)), initial conditions close enough to zero lead to solutions which converge to zero (solid line), while initial conditions far enough from zero lead to solutions which grow without bound (dashed line). After the bifurcation (fig. 14(b)), initial conditions close enough to zero lead to solutions which converge to a limit cycle (solid line), while initial conditions which are far enough from zero still lead to solutions which grow without bound (dashed line). This suggests that a large amplitude unstable limit cycle surrounds the stable limit cycle. The behaviour close to zero is consistent with the prediction of our centre manifold analysis: a stable limit cycle is created by the supercritical Hopf bifurcation. The unstable limit cycle is not predicted by our centre manifold analysis, but is consistent with theoretical predictions of what may occur near a point in parameter space where the criticality of a Hopf bifurcation changes [24, Section 7.1],[26],[27].

Let us now consider the points where the criticality switches in more detail. At such points, the coefficient a is 0, which means that the cubic terms of the nonlinearity do not

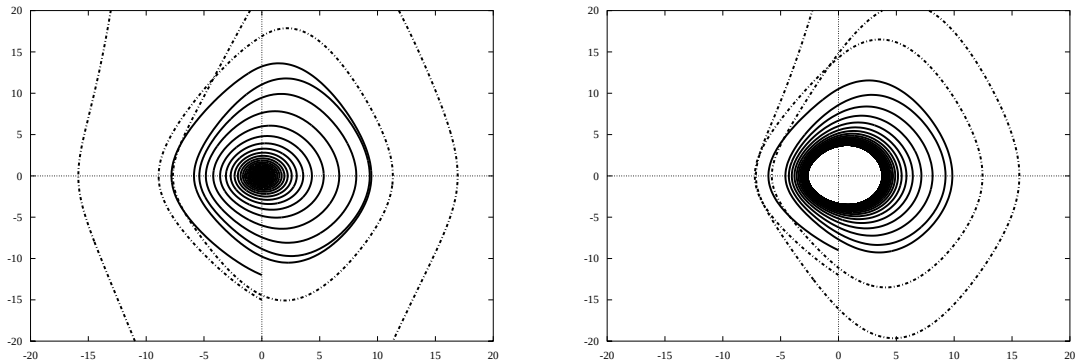

FIG. 14: Numerical simulations of (12) illustrating a supercritical Hopf bifurcation for the traditional vibration mode, close to the point of change in criticality. Shown is $\dot{\eta}$ vs η for two different initial conditions. Parameter values: $\beta = 0.1, \gamma = 0.1, 1/T = 0.4, p_0 = 0.8, p_1 = 0.2, p_2 = 0.1, \theta = 0$. (a) Before Hopf bifurcation, $t_1 = 5$. (b) After Hopf bifurcation, $t_1 = 7$.

determine the behaviour of the system. It has been shown [26, 27] that from such points there emerges a secondary bifurcation curve, which is a saddle-node bifurcation of limit cycles. This branch may either result in a large amplitude stable limit cycle surrounding the unstable limit cycle produced by the subcritical part of the Hopf bifurcation curve or a large amplitude unstable limit cycle surrounding the stable limit cycle produced by the supercritical part of the Hopf bifurcation curve. The numerical simulations of figure 14 appear to fall into the latter category.

To investigate this phenomenon further, we performed numerical continuations of the periodic solutions of our system, using the package DDE-BIFTOOL [13]. Among other things, this package allows one to find periodic solutions of delay differential equations, calculate their stability and determine how this changes as parameters are varied. Fig. 15 shows the results of numerically continuing the branch of periodic solutions produced by the Hopf bifurcation when $\beta = 0.1$, for both the traditional and axial-torsional cases. The curves plot the maximum amplitude of η for the periodic solution as a function of t_1. For the traditional case we show continuations for three different values of T. Recall that the trivial solution is stable for t_1 less than the Hopf bifurcation value in this case. Thus one can see the transition from subcritical ($1/T = 1/3$) to supercritical with an additional large amplitude unstable limit cycle ($1/T = 0.387$) to supercritical ($1/T = 0.445$). This confirms the results of the numerical simulations of fig. 14. Continuations for other values

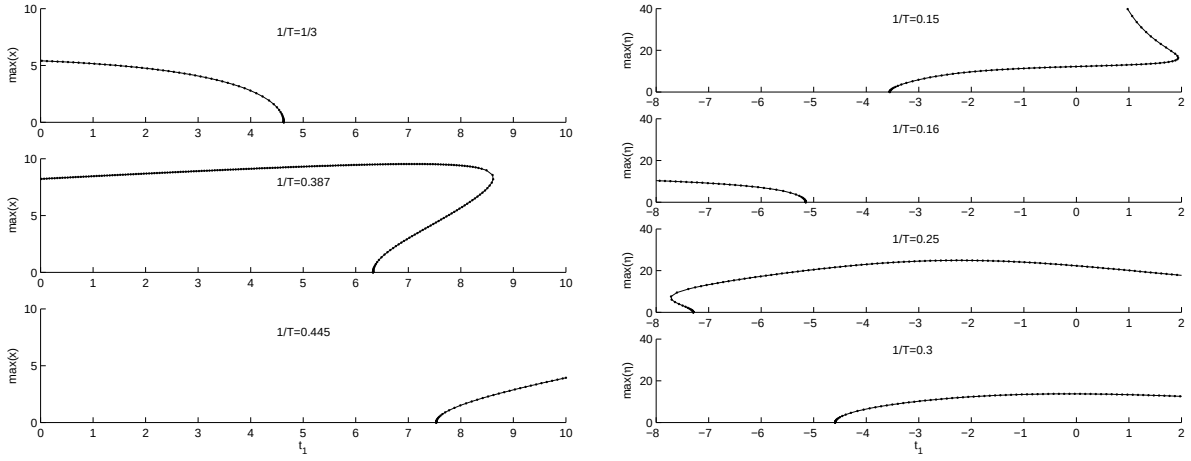

(a) (b)

FIG. 15: Numerical continuation of branches of periodic solutions from the Hopf bifurcation when $\beta = 0.1$. Other parameter values are (a) $p_0 \cos(\theta) = -0.8$, $\tilde{p}_1 = -0.2$, $\tilde{p}_2 = -0.1$, $\gamma = 0.1$; (b) $p_0 \cos(\theta) = -0.8$, $\tilde{p}_1 = -0.2$, $\tilde{p}_2 = -0.1$, $\gamma = 0.1$. The curves show the maximum amplitude of η on the periodic solution as a function of t_1 for the given value of $1/T$. (a) Traditional case. (b) Axial-torsional case.

of $1/T$ were similar to these: values of $1/T$ where the Hopf bifurcation is subcritical produce branches like fig. 15(a) top, places where the Hopf bifurcation is supercritical and $1/T < 0.4$ produce branches like fig. 15(a) middle, for $1/T > 0.4$ the bifurcation is supercritical and numerical continuations produce branches like fig. 15(a) bottom. For the axial-torsional case, we show continuations for four values of $1/T$. Recall that the trivial solution is stable for t_1 greater than the Hopf bifurcation value in this case. Here one sees the changes in the periodic solution branches near two different criticality switches on fig. 13, at $1/T \approx 0.155$ and $1/T \approx 0.28$. Specifically, at $1/T = 0.15$ the Hopf bifurcation is subcritical with an additional large amplitude limit cycle, at $1/T = 0.16$ it is subcritical, at $1/T = 0.25$ it is supercritical with an additional large amplitude limit cycle and at $1/T = 0.3$ it is subcritical. Thus the axial-torsional case exhibits both types of behaviour associated with switches of criticality.

DISCUSSION AND CONCLUSIONS

For the purposes of machining, system parameters that can be varied easily are cutting width, thickness and cutting speed. We illustrate the effect of varying thickness and speed with linear stability boundaries in the $(1/T, t_1)$ plane, and consider the way this changes with varying cutting width. While the standard analysis of the delay differential equation that describes chatter in metal cutting shows similar stability lobes, they are created by varying the cutting width.

Adding nonlinear forcing due to nonlinear friction on the rake face of the tool, and introducing varying angle of vibration generates significantly different stability lobes that usually studied, most easily seen is the presence of closed loops. This, while interesting mathematically, is not as pertinent as the effect of varying vibration angle on the whole picture, which leads to such observations as the frequency of induced vibration must be less than the natural frequency of the axial-torsional mode, and the reverse for the traditional vertical vibration mode. Close to the boundaries either a stable or unstable limit cycle will exist, and the nonlinear stability analysis we perform here uncovers this distinction. We find that the traditional case is supercritical for large cutting speed, with several switches between super- and subcritical for smaller cutting speeds. The axial-torsional case also has switches between super- and subcritical, but these all occur for negative values of t_1, thus the Hopf bifurcation is always subcritical for physically reasonable values of t_1.

The switch from sub- to supercritical bifurcation along a boundary indicates a degeneracy in the Hopf coefficient, meaning that higher order terms are needed to determine the stability at that point. A numerical continuation package can give some indication of global picture during these transitions, however, and we see a saddle node bifurcation of the limit cycle occurs at intermediate parameter values. This is validated by numerical simulations of the DDE which show a stable limit cycle enclosed by an unstable cycle for appropriate parameter values in the traditional case.

Numerical continuation can also show that phenomena that occur for nonphysical parameter values influences the behaviour for physically relevant parameter values. The most striking example we found is a situation where linear stability analysis indicates the equilibrium solution is stable for $t_1 > 0$, i.e. all physically reasonable values of the cutting thickness. Since the stability boundary and associated Hopf bifurcation lie in the region $t_1 < 0$, one might assume that it has no influence on the behaviour of the physical system. However, numerical continuations show that unstable periodic solutions which are generated by Hopf bifurcations for $t_1 < 0$ persist when $t_1 > 0$ and thus can affect the

behaviour of the physical system.

The implications of switching from a supercritical to subcritical Hopf from a machining stand-point concern the accuracy of the stability boundaries in the linear stability diagram. When a supercritical Hopf is encountered the linear stability boundary determines where the steady cutting solution goes unstable, but if the Hopf is subcritical, the existence of the small unstable cycle near the steady cutting solution means that small perturbations could push the trajectory out past the cycle and into a region of instability. Noise in the system then will blur boundaries, rendering them much less accurate.

This study suggests further mathematical investigation of the global bifurcations of such DDE systems, which would be needed to fully explain the switching behaviour seen in fig. 15. The theory of global bifurcation in DDEs with a constant delay term has not been mapped out, and the development of such a framework would be a significant advance in the understanding on nonlinear DDEs.

Acknowledgements

This research was supported by the Natural Sciences and Engineering Research Council of Canada (grant no. 171089) and by the NSF-EPSCoR program at the University of Montana.

[1] Stone, E., and Askari, A., 2002. "Nonlinear Models of Chatter in Drilling Processes". *Dynamical Systems,* **17**(1), pp. 65–85.

[2] Stone, E., and Campbell, S. A., 2004. "Stability and Bifurcation Analysis of a Nonlinear DDE Model for Drilling". *J. Nonlinear Science,* **14**(1), pp. 27–57.

[3] Tlusty, J., 1986. "The Dynamics of High-Speed Milling". *J. Eng. Ind.,* **108**, pp. 59–67.

[4] Altintas, Y., and Budak, E., 1995. "Analytical Prediction of Stability Lobes in Milling". *Annals of the CIRP,* **44**(1), pp. 357–362.

[5] Bayly, P. V., Metzler, S. A., Schaut, A. J., and Young, K. A., 2001. "Theory of Torsional Chatter in Twist Drills: Model, Stability Analysis and Comparison to Test". *ASME J. Man. Sci. & Eng.,* **123**, pp. 552–561.

[6] Bayly, P. V., Young, K. A., and Halley, J. E., 2001. "Analysis of Tool Oscillation and Hole Roundness Error in a Quasi-Static Model of Reaming". *ASME J. Man. Sci. & Eng.,* **123**, pp. 387–396.

[7] Stépán, G., 1989. *Retarded Dynamical Systems: Stability and Characteristic Functions.* Longman Group, Essex.

[8] Stépán, G., 1998. "Delay-Differential Equation Models for Machine Tool Chatter". In *Dynamics and Chaos in Manufacturing Processes*, F. Moon, ed. J. Wiley, New York, pp. 165–191.

[9] Campbell, S. A., and Bélair, J., 1995. "Analytical and Symbolically-Assisted Investigation of Hopf Bifurcations in Delay-Differential Equations". *Can. Appl. Math. Quart.,* **3**(2), pp. 137–154.

[10] Faria, T., and Magalhães, L., 1995. "Normal Forms for Retarded Functional Differential Equations with Parameters and Applications to Hopf Bifurcation". *JDE,* **122**, pp. 181–200.

[11] Hale, J. K., 1985. "Flows on Center Manifolds for Scalar Functional Differential Equations". *Proc. Roy. Soc. Edinburgh,* **101A**, pp. 193–201.

[12] Wischert, W., Wunderlin, A., Pelster, A., Olivier, M., and Groslambert, J., 1994. "Delay-Induced Instabilities in Nonlinear Feedback Systems". *Phys. Rev. E,* **49**(1), pp. 203–219.

[13] Engelborghs, K., Luzyanina, T., and Samaey, G., 2001. "DDE-BIFTOOL v. 2.00: a Matlab Package for Bifurcation Analysis of Delay Differential Equations.". Tech. Rep. TW-330, Department of Computer Science, K.U. Leuven, Leuven, Belgium.

[14] Tobias, S. A., 1965. *Machine Tool Vibration.* J. Wiley, New York.

[15] Bhatt, S. J., and Hsu, C. S., 1966. "Stability Criteria for Second Order Dynamical Systems with Time Lag.". *J. App. Mech.,* **33**, pp. 113–118.

[16] Campbell, S. A., 1999. "Stability and Bifurcation in the Harmonic Oscillator with Multiple Delayed Feedback Loops.". *Dyn. Cont. Disc. Impul. Sys.,* **5**, pp. 225–235.

[17] Campbell, S. A., Bélair, J., Ohira, T., and Milton, J., 1995. "Limit Cycles, Tori, and Complex Dynamics in a Second-Order Differential Equations with Delayed Negative Feedback". *J. Dyn. Diff. Eqs.,* **7**(1), pp. 213–236.

[18] Cooke, K. L., and Grossman, Z., 1982. "Discrete Delay, Distributed Delay and Stability Switches". *J. Math. Anal. Appl.,* **86**, pp. 592–627.

[19] Hsu, C. S., and Bhatt, S. J., 1966. "Stability Charts for Second-Order Dynamical Systems with Time Lag.". *J. Appl. Mech.,* **33**, pp. 119–124.

[20] Merchant, M. E., 1945. "Mechanics of the Cutting Process. I. Orthogonal Cutting and a Type 2 Chip". *J. Appl. Phys.,* **16**, pp. 267–275.

[21] Oxley, P. L. B., 1989. *The Mechanics of Machining: an Analytical Approach to Assessing Machinability.* Ellis Horwood, Chichester, England.

[22] Hale, J. K., and Verduyn Lunel, S. M., 1993. *Introduction to Functional Differential Equations.* Springer Verlag, New York.

[23] Kolmanovskii, V. B., and Nosov, V. R., 1986. *Stability of Functional Differential Equations.* Academic Press, London, England.

[24] Guckenheimer, J., and Holmes, P. J., 1993. *Nonlinear Oscillations, Dynamical Systems and Bifurcations of Vector Fields.* Springer-Verlag, New York.

[25] Ermentrout, G. B., 2002. *Simulating, Analyzing and Animating Dynamical Systems: A Guide to XPPAUT for Researcher and Students.* SIAM, Philadelphia, PA.

[26] Golubitsky, M., and Langford, W. F., 1981. "Classification and Unfoldings of Degenerate Hopf Bifurcation". *JDE,* **41**, pp. 525–546.

[27] Takens, F., 1973. "Unfoldings of Certain Singularities of Vector Fields: Generalized Hopf Bifurcations". *JDE,* **14**, pp. 476–493.